τ_0 and higher L_D (submicrometer) (Fig. 1C). From the linear absorption coefficients (Fig. 2A), the absorption lengths are $L_\alpha \sim 100$ nm (at $\lambda = 500$ nm). These conservatively estimated carrier diffusion lengths measured in $CH_3NH_3PbI_3$ are comparable to the optical absorption lengths for $\lambda \leq 500$ nm but are shorter than the absorption lengths at longer wavelengths. Increasing the optical thickness of these layers through light-trapping architectures compensates for this slight mismatch, accounting for the high photoconversion efficiencies reported in these systems (*9*–*14*, *40*).

References and Notes

1. P. M. Beaujuge, J. M. J. Fréchet, *J. Am. Chem. Soc.* **133**, 20009–20029 (2011).
2. A. Facchetti, *Chem. Mater.* **23**, 733–758 (2011).
3. R. S. Selinsky, Q. Ding, M. S. Faber, J. C. Wright, S. Jin, *Chem. Soc. Rev.* **42**, 2963–2985 (2013).
4. H. Sirringhaus, *Adv. Mater.* **17**, 2411–2425 (2005).
5. H. A. Atwater, A. Polman, *Nat. Mater.* **9**, 205–213 (2010).
6. B. Wu *et al.*, *Nat. Commun.* **4**, 2004 (2013).
7. B. O'Regan, M. Grätzel, *Nature* **353**, 737–740 (1991).
8. A. Yella *et al.*, *Science* **334**, 629–634 (2011).
9. J. Burschka *et al.*, *Nature* **499**, 316–319 (2013).
10. H. S. Kim *et al.*, *Sci. Rep.* **2**, 591 (2012).
11. J. H. Heo *et al.*, *Nat. Photonics* **7**, 486–491 (2013).
12. M. M. Lee, J. Teuscher, T. Miyasaka, T. N. Murakami, H. J. Snaith, *Science* **338**, 643–647 (2012); 10.1126/science.1228604.
13. L. Etgar *et al.*, *J. Am. Chem. Soc.* **134**, 17396–17399 (2012).
14. J. M. Ball, M. M. Lee, A. Hey, H. J. Snaith, *Energy Environ. Sci.* **6**, 1739 (2013).
15. W. J. E. Beek, M. M. Wienk, R. A. J. Janssen, *Adv. Funct. Mater.* **16**, 1112–1116 (2006).
16. J. K. J. van Duren *et al.*, *Adv. Funct. Mater.* **14**, 425–434 (2004).
17. J. Piris *et al.*, *J. Phys. Chem. C* **113**, 14500–14506 (2009).
18. Y. Kim *et al.*, *J. Mater. Sci.* **40**, 1371–1376 (2005).
19. Y. Kim *et al.*, *J. Phys. Chem. C* **111**, 8137–8141 (2007).
20. J. H. Im, C. R. Lee, J. W. Lee, S. W. Park, N. G. Park, *Nanoscale* **3**, 4088–4093 (2011).
21. P. E. Shaw, A. Ruseckas, I. D. W. Samuel, *Adv. Mater.* **20**, 3516–3520 (2008).
22. A. Haugeneder *et al.*, *Phys. Rev. B* **59**, 15346–15351 (1999).
23. J. E. Kroeze, T. J. Savenije, M. J. W. Vermeulen, J. M. Warman, *J. Phys. Chem. B* **107**, 7696–7705 (2003).
24. R. R. Lunt, J. B. Benziger, S. R. Forrest, *Adv. Mater.* **22**, 1233–1236 (2010).
25. H. Najafov, B. Lee, Q. Zhou, L. C. Feldman, V. Podzorov, *Nat. Mater.* **9**, 938–943 (2010).
26. P. Peumans, A. Yakimov, S. R. Forrest, *J. Appl. Phys.* **93**, 3693 (2003).
27. D. Zhitomirsky, O. Voznyy, S. Hoogland, E. H. Sargent, *ACS Nano* **7**, 5282–5290 (2013).
28. V. I. Klimov, *Annu. Rev. Phys. Chem.* **58**, 635–673 (2007).
29. G. N. Ostojic *et al.*, *Phys. Rev. Lett.* **94**, 097401 (2005).
30. G. Grancini *et al.*, *Nat. Mater.* **12**, 29–33 (2013).
31. G. Grancini *et al.*, *J. Phys. Chem. Lett.* **3**, 517–523 (2012).
32. A. A. Bakulin, J. C. Hummelen, M. S. Pshenichnikov, P. H. M. Van Loosdrecht, *Adv. Funct. Mater.* **20**, 1653–1660 (2010).
33. M. L. Mueller, X. Yan, B. Dragnea, L. S. Li, *Nano Lett.* **11**, 56–60 (2011).
34. Typically, PB peaks in TAS can arise from Coulomb interaction or state filling of the quasi-particles. In the former case, coulombic interaction among the excitons gives rise to a shift in energy of the probe beam–induced transitions, which occur in the vicinity of the excitons generated by the earlier pump beam. Such a phenomenon is commonly observed in quantum-confined low-dimensional systems or under high fluence excitation. In this mechanism, the occurrence of the PB peaks usually coincides with the occurrence of adjacent photoinduced absorption peaks because of the shift or broadening of the absorption peak. Furthermore, the PB peak positions will also shift with increasing pump fluence. The absence of photoinduced absorption peaks or pump fluence dependence of the PB peaks in these $CH_3NH_3PbI_3$ films allows us to rule out Coulomb interaction. On the other hand, state filling arises because of the changes in population of the various electronic states brought about by the initial pump beam. Hence, it will only influence probe beam–induced transitions that involve electronic states with changed populations.
35. A. E. Jailaubekov *et al.*, *Nat. Mater.* **12**, 66–73 (2013).
36. T. Baikie *et al.*, *J. Mater. Chem. A* **1**, 5628 (2013).
37. C. R. Kagan, D. B. Mitzi, C. D. Dimitrakopoulos, *Science* **286**, 945–947 (1999).
38. D. B. Mitzi, S. Wang, C. A. Feild, C. A. Chess, A. M. Guloy, *Science* **267**, 1473–1476 (1995).
39. P. W. M. Blom, V. D. Mihailetchi, L. J. A. Koster, D. E. Markov, *Adv. Mater.* **19**, 1551–1566 (2007).
40. W. Zhang *et al.*, *Nano Lett.* **13**, 4505–4510 (2013).

Acknowledgments: The authors thank M. Duchamp and C. Boothroyd from Ernst Ruska-Centrum, Forschungszentrum Jülich, Germany, for the FIB and transmission electron microscopy work carried out. Financial support from NTU startup grant M4080514, School of Physical and Mathematical Sciences collaborative research award M4080536, Singapore National Research Foundation through the Competitive Research Program (NRF-CRP4-2008-03), and the Singapore-Berkeley Research Initiative for Sustainable Energy (SinBeRISE) program is gratefully acknowledged. M.G. thanks the European Research Council for financial support under the Advanced Research Grant (ARG 247404) "Mesolight."

Supplementary Materials

www.sciencemag.org/content/342/6156/344/suppl/DC1
Materials and Methods
Fig. S1 to S9
Table S1
References (*41*, *42*)

12 July 2013; accepted 4 September 2013
10.1126/science.1243167

Product-to-Parent Reversion of Trenbolone: Unrecognized Risks for Endocrine Disruption

Shen Qu,[1] Edward P. Kolodziej,[2]* Sarah A. Long,[3] James B. Gloer,[3] Eric V. Patterson,[4] Jonas Baltrusaitis,[5,6] Gerrad D. Jones,[2] Peter V. Benchetler,[2] Emily A. Cole,[2] Kaitlin C. Kimbrough,[2] Matthew D. Tarnoff,[1] David M. Cwiertny[1,7]*

Trenbolone acetate (TBA) is a high-value steroidal growth promoter often administered to beef cattle, whose metabolites are potent endocrine-disrupting compounds. We performed laboratory and field phototransformation experiments to assess the fate of TBA metabolites and their photoproducts. Unexpectedly, we observed that the rapid photohydration of TBA metabolites is reversible under conditions representative of those in surface waters (pH 7, 25°C). This product-to-parent reversion mechanism results in diurnal cycling and substantial regeneration of TBA metabolites at rates that are strongly temperature- and pH-dependent. Photoproducts can also react to produce structural analogs of TBA metabolites. These reactions also occur in structurally similar steroids, including human pharmaceuticals, which suggests that predictive fate models and regulatory risk assessment paradigms must account for transformation products of high-risk environmental contaminants such as endocrine-disrupting steroids.

Humans discharge a multitude of bioactive organic contaminants into receiving waters that adversely affect aquatic organisms (*1*–*3*). Risk assessment approaches for regulating these contaminants often are simplistic, typically assuming that if degradation occurs, the associated ecological risk greatly decreases. However, there is growing sentiment that some environmental transformation reactions result in minimal mitigation of risk, forming products that retain bioactive moieties, exhibit greater toxicity, or affect different biological end points (*4*, *5*).

The androgenic steroid trenbolone acetate [TBA; 17β-(acetyloxy)estra-4,9,11-trien-3-one] is an anabolic growth promoter implanted in over 20 million cattle annually (*6*, *7*), with annual revenue attributable to its use likely exceeding $1 billion (*8*). Given the extensive use of TBA, its dominant metabolite [17α-trenbolone (17α-TBOH)] and other known metabolites

[1]Department of Civil and Environmental Engineering, University of Iowa, 4105 Seamans Center for the Engineering Arts and Sciences, Iowa City, IA 52242–1527, USA. [2]Department of Civil and Environmental Engineering, University of Nevada, Reno, Mail Stop 258, Reno, NV 89557, USA. [3]Department of Chemistry, University of Iowa, Iowa City, IA 52242–1527, USA. [4]Department of Chemistry, Truman State University, Kirksville, MO 63501, USA [5]PhotoCatalytic Synthesis Group, MESA+ Institute for Nanotechnology, Faculty of Science and Technology, University of Twente, Meander 225, Post Office Box 217, 7500 AE Enschede, Netherlands. [6]Department of Occupational and Environmental Health, College of Public Health, University of Iowa, Iowa City, IA 52242, USA. [7]Department of Chemical and Biochemical Engineering, University of Iowa, 4133 Seamans Center for the Engineering Arts and Sciences, Iowa City, IA 52242–1527, USA.

*Corresponding author. E-mail: koloj@unr.edu (E.P.K.); david-cwiertny@uiowa.edu (D.M.C.)

[17β-trenbolone (17β-TBOH) and trendione (TBO)] can be widespread in agricultural environments (*9*, *10*). 17α-TBOH and 17β-TBOH are potent endocrine-disrupting compounds, with concentrations as low as 10 to 30 ng/liter causing skewed sex ratios and reduced fecundity in fish (*7*, *11*). Nevertheless, observations of TBA metabolite occurrence have not yet translated to concern, because they are believed to exhibit limited persistence in receiving waters. For example, manufacturer studies used for regulatory approvals specifically point to limited ecosystem risks of TBA metabolites due to rapid photodegradation (*12*).

Accordingly, we previously identified the structure and bioactivity of TBA metabolite photoproducts, showing that 17β-TBOH undergoes rapid photohydration (*13*) to yield 12,17-dihydroxyestra-5(10),9(11)-diene-3-one (or simply 12-hydroxy-17β-TBOH) (*14*, *15*). An analogous C12-hydroxylated photoproduct was identified for TBO (*15*), whereas 17α-TBOH yields both major C12 [12-hydroxy-17α-TBOH (*15*)] and minor C5 (5-hydroxy-17α-TBOH) hydroxylated photoproducts (supplementary text and figs. S1 and S2). Because these photoproduct mixtures retained bioactivity (*15*), we focused on photoproduct stability across a range of conditions representative of light (day) and dark (night) surface waters. When photoproduct transformation was observed, we used liquid chromatography high-resolution tandem mass spectroscopy (LC-HRMS/MS) and nuclear magnetic resonance (NMR) to characterize the resulting product structures and the potential for persistent bioactivity in surface waters (*16*).

Simulated day-night cycling experiments conducted over 72 hours at pH 7, 25°C revealed unexpected persistence of TBA metabolites (Fig. 1A). For example, 17α-TBOH decay during irradiation was consistently followed by concentration rebound during subsequent dark periods, with equivalent rates of photodecay and dark regeneration for each diurnal cycle. Both NMR (figs. S3 to S10) and LC-HRMS/MS confirmed that 17α-TBOH was regenerated in the dark. This dynamic behavior appears to be linked to the thermal (i.e., nonphotochemical) instability of C5 and C12 hydroxylated photoproducts, which decayed concurrently with 17α-TBOH regrowth.

A noteworthy feature of both 5- and 12-hydroxy-17α-TBOH is their allylic alcohol moiety (Fig. 1A). Steroidal allylic alcohols are prone to dehydration but typically under more aggressive conditions (e.g., low pH and high temperature) (*17*). However, our data suggest that 5- and 12-hydroxy-17α-TBOH dehydrate under ambient conditions, with the driving force being regeneration of the conjugated trienone system. This coupled photohydration-dehydration mechanism results in net reversibility of 17α-TBOH photolysis, a product-to-parent reversion mechanism also observed for other TBA metabolites (Fig. 1B). 17β-TBOH and TBO exhibited reduced regrowth during 12-hour dark periods (~1% of initial mass) relative to 17α-TBOH (~15%), which we attribute to their photoproducts being more susceptible to concurrent phototransformation and hydroxylation rather than dehydration (supplementary text and fig. S11).

We also simulated TBA metabolite transport from the photic zone of surface water into darker regions (such as lake hypolimnia, hyporheic zones, or benthic sediments) by photolyzing TBA metabolite solutions to >99% transformation (pH 7, 6 hours irradiation) and then storing the resulting photoproduct mixtures in the dark for 5 days at 25°C. Consistent with the diurnal cycling experiments, 17α-TBOH exhibited substantial reversion, with over 60% of its initial mass recovered after 120 hours, whereas 17β-TBOH and TBO yielded 10% recovery over this period (Fig. 2A).

The rates and extents of product-to-parent reversion were highly dependent on solution conditions, with some promoting rapid and near-complete TBA metabolite regeneration. For example, 88 ± 3% of the initial 17α-TBOH mass was regenerated nearly instantaneously when photoproduct mixtures were acidified to pH 2, with slightly lower recoveries (66 ± 5%) when raised to pH 12 (Fig. 2A). Reversion of 17β-TBOH and TBO was also acid-catalyzed (65 ± 7% and 32 ± 4% recovery, respectively), but their regrowth was more limited at pH 12. We believe that these recoveries at pH 2 probably reflect the maximum photoproduct mass available for reversion.

The reversion of 17α-TBOH was also enhanced at pH 9 and pH 5, at least initially, relative to pH 7 (Fig. 2B). Thus, acid- and base-catalyzed reversion will probably result in higher 17α-TBOH concentrations in mildly acidic or alkaline waters. In fact, the initial rate of reversion at pH 5 is fast enough to slow 17α-TBOH phototransformation relative to the rate observed at neutral pH (supplementary text and fig. S12). In manufacturer regulatory studies, slower rates of 17α-TBOH phototransformation at pH 5 relative to pH 7 were attributed, we believe incorrectly, to variations in solar irradiance from cloudy weather experienced during data collection at pH 5 (*12*).

Reversion is also temperature-dependent. At pH 7, rates of 17α-TBOH regrowth increased nearly 30-fold from 5° to 35°C (Fig. 2C), a temperature range representative of seasonal variations. Faster reversion rates at 35°C ultimately allowed more complete 17α-TBOH recovery in the dark (30% over 12 hours and 75% over 60 hours). Accordingly, we expect photoproduct-to-parent reversion to be most prominent in warm sunlit waters, whereas colder winterlike conditions

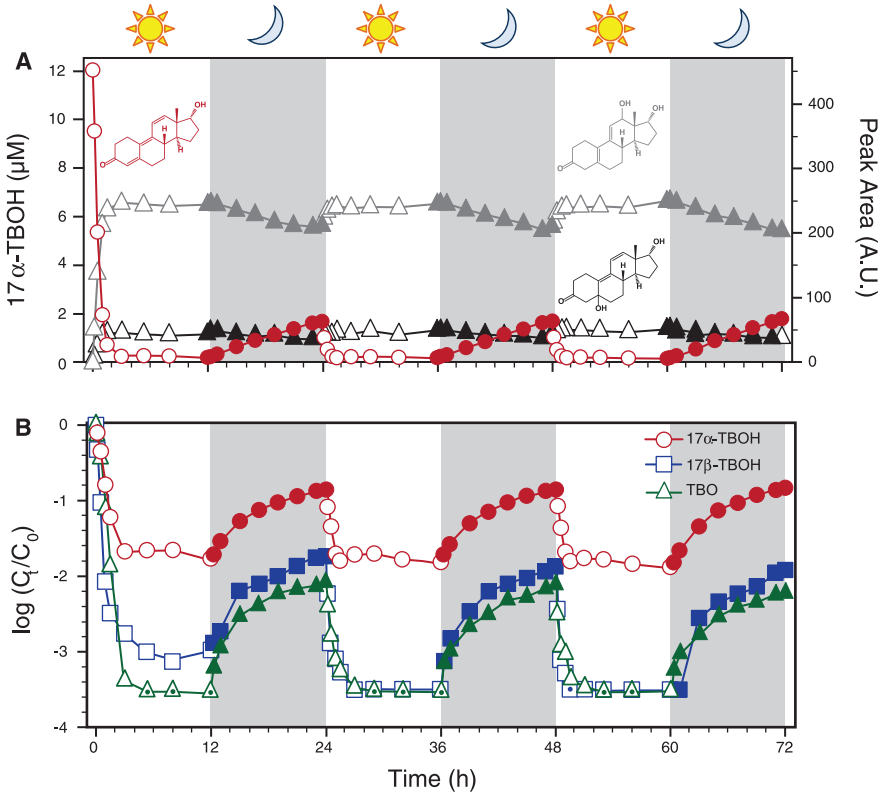

Fig. 1. Diurnal cycling of TBA metabolites. (**A**) Day-night cycling of 17α-TBOH (red), 12-hydroxy-17α-TBOH (gray), and 5-hydroxy-17α-TBOH (black) at pH 7, 25°C. Data for 17α-TBOH are presented as aqueous concentration (left axis), whereas peak areas from spectrophotometric absorbance [wavelength (λ) = 350 nm for 17α-TBOH; λ = 254 nm for photoproducts] are also presented (right axis). (**B**) Corresponding data for 17β-TBOH and TBO, where symbols with a center dot indicate values below our detection limit. In these cases, data points correspond to this limit (~3 nM) for 17β-TBOH and TBO. C_t/C_0, time-dependent concentration normalized to initial concentration; h, hours; A.U., arbitrary units.

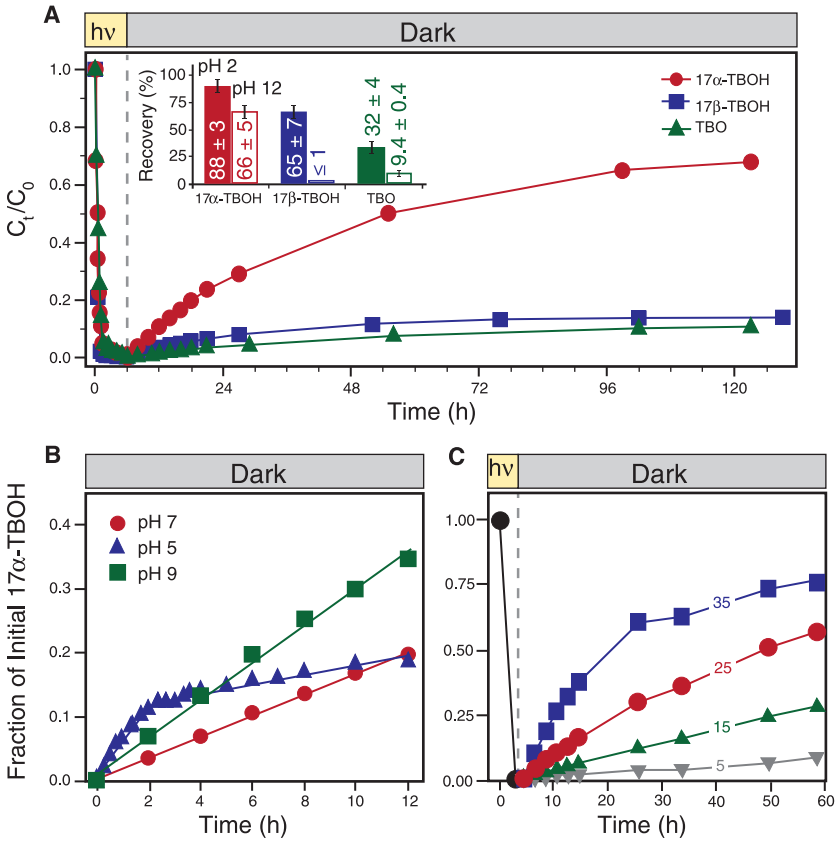

Fig. 2. Dark regrowth of TBA metabolites and the influence of pH and temperature on reversion. (**A**) Regeneration of 17α-TBOH, 17β-TBOH, and TBO in photoproduct mixtures stored in the dark (pH 7, 25°C). hν, light energy. The inset reports the percent recovery (mean and standard deviation of triplicate analyses) when photoproduct mixtures were adjusted to pH 2 or pH 12. Also shown is the regeneration of 17α-TBOH as a function of (**B**) pH (5, 7, and 9 at 25°C) and (**C**) temperature (5, 15, 25, and 35°C at pH 7) from photoproduct mixtures. In (B), the initial rate of regrowth obtained from linear regression analysis was enhanced at pH 9 (0.3 μM $hour^{-1}$) and, at least initially [time (*t*) < 2 hours], at pH 5 (0.6 μM $hour^{-1}$) relative to pH 7 (0.17 μM $hour^{-1}$). The slower rate observed over longer time scales at pH 5 (0.07 μM $hour^{-1}$) probably reflects differences in the dehydration rates of 5- and 12-hydroxy-17α-TBOH.

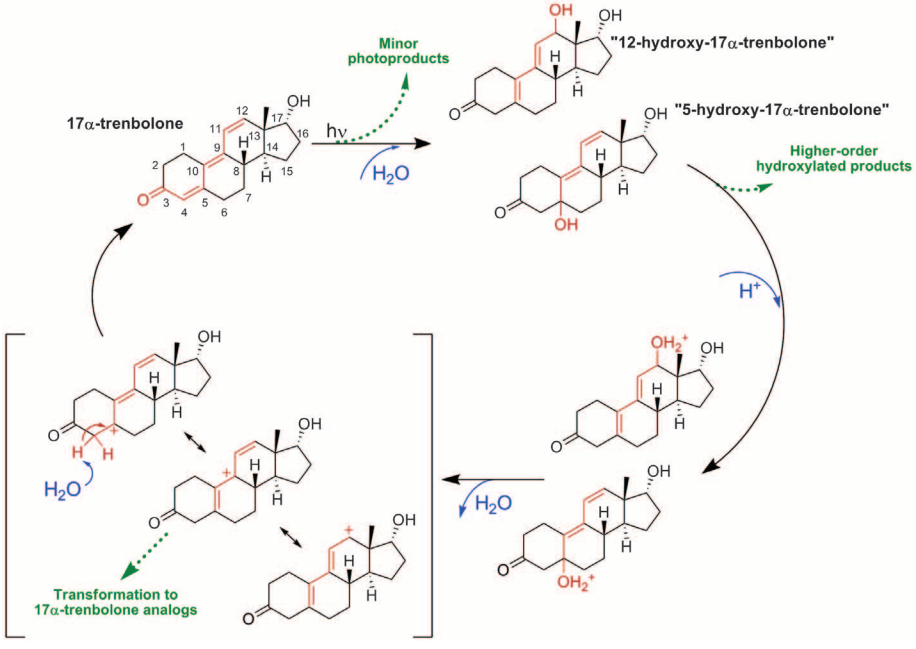

Fig. 3. Proposed acid-catalyzed reversible photohydration of 17α-TBOH. Dashed green arrows indicate pathways that break the product-to-parent reversion cycle. Red highlights detail the changes in the trienone structure during photolysis and subsequent dehydration.

should promote photoproduct stability by slowing dehydration.

Accounting for these effects, we can now present a more complete characterization of TBA metabolite fate in surface waters. Consistent with established pathways for allylic sterols (*17*), we propose that dehydration at moderately acidic to low pH proceeds via unimolecular (E1) elimination involving the formation of a resonance-stabilized carbocation (Fig. 3). Parent regeneration from this carbocation intermediate may be accompanied by concurrent transformations, including structural rearrangements and/or reaction with naturally abundant nucleophiles, to yield complex mixtures of isomers, structural analogs, and substituted derivatives of TBA metabolites with uncharacterized bioactivity. For example, while monitoring TBO photoproduct reversion at pH 5, we observed evidence of photoproduct interconversion and formation of a presumed structural analog that coelutes with TBO (supplementary text and figs. S13 to S18). These phenomena were not observed at neutral or basic pH, which is consistent with the proposed acid-promoted carbocation intermediate. At neutral and basic pH, dehydration is more likely to proceed via enol or enolate formation in parallel to reactions yielding higher-order hydroxylated products.

Beyond model laboratory systems, we have also observed reversion in more complex aquatic matrices, including Iowa River water (Fig. 4), as well as in experiments using environmentally relevant TBA metabolite concentrations (for example, ~420 ng/liter 17β-TBOH; fig. S19). To explore reversion in agricultural receiving waters with competing attenuation pathways (such as sorption and biodegradation), we dosed a small collection pond on a rangeland with manure from TBA-implanted cattle (supplementary text). After overnight leaching increased 17α-TBOH concentrations in the pond to 6.1 ng/liter, concentrations decreased by ~50% during the day, consistent with phototransformation. At sunset, a large (31-liter) sample was collected and processed so that

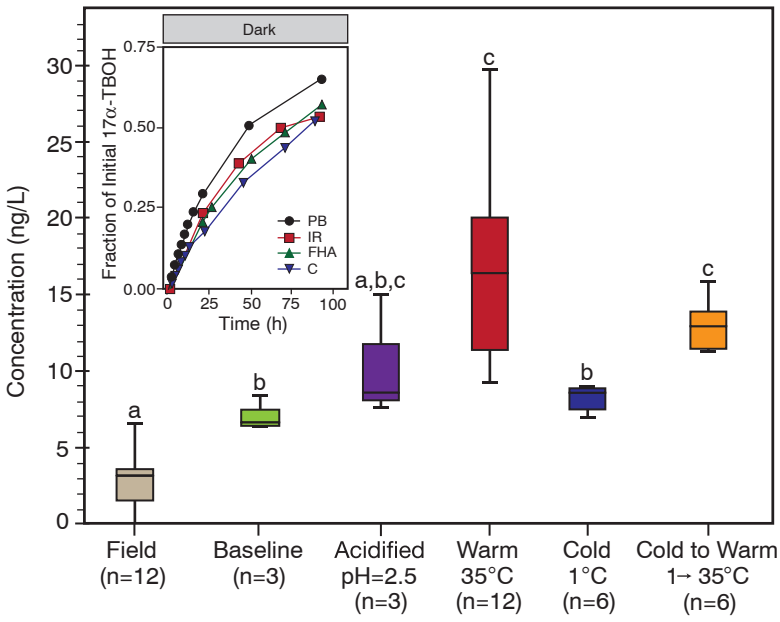

Fig. 4. 17α-TBOH dynamics in a field mesocosm and complex aquatic matrices. After dosing the collection pond (at 22:00), field samples (n = 4, in triplicate) were analyzed over 17 hours. At sunset (15:00), the baseline sample was processed and split into subsamples, which were either acidified to pH 2.5, incubated [warm, temperature (T) = 35°C], refrigerated (cold, T = 1°C), or refrigerated then incubated after 24 hours (cold to warm, T = 1° → 35°C). Group means are different [one-way analysis of variance: $F(5,37) = 17.5$, $P < 0.001$] if groups do not share the same letter as other groups (Games-Howell post-hoc test: $P < 0.05$). Lines, boxes, and whiskers represent median, interquartile, and minimum and maximum values, respectively. The inset shows regeneration of 17α-TBOH in photoproduct mixtures (dark, 25°C) in solutions of 10 mg/liter Fluka Humic Acid (FHA), 250 mg/liter of bicarbonate as $CaCO_3$ (C), and Iowa River water (IR; turbidity, 15.1 nephelometric turbidity units; alkalinity, 196 mg/liter as $CaCO_3$; total hardness, 270 mg/liter as $CaCO_3$; total dissolved organic carbon, 16.6 mg/liter; pH 8.2.). Provided for comparison are data from a phosphate buffer (PB) system. Unless noted, all systems were at pH 7. The rate of reversion is less in Iowa River water than would be expected for its alkaline pH, probably because of the slight inhibition observed in model systems with Fluka Humic Acid and bicarbonate.

subsamples of this baseline sample could be subjected to different storage conditions (Fig. 4). Laboratory storage at 35°C significantly increased 17α-TBOH concentrations (from 7 to 20 ng/liter; Games-Howell post-hoc test, $P = 0.003$), whereas samples stored at 1°C were statistically identical to the baseline sample (Games-Howell post-hoc test, $P = 0.65$). However, when the temperature of these 1°C samples was subsequently raised after 24 hours to 35°C, 17α-TBOH concentrations statistically increased to 15 ng/liter (Games-Howell post-hoc test, $P = 0.005$). These data are consistent with expected trends for product-to-parent reversion dynamics under actual field conditions. Incidentally, we also observed similar decay and regrowth characteristics for a major uncharacterized, nontarget compound, probably steroidal, in our gas chromatography–tandem mass spectrometry chromatograms, whose occurrence was highly correlated to known TBA metabolites (figs. S20 to S22).

Although growth-promoting steroids provide indisputable economic and environmental advantages (such as reduced land use, nutrient loads, and greenhouse gas emissions) for animal agriculture (*18*), their use should not compromise environmental health. Contrary to prevailing assumptions of limited environmental persistence, product-to-parent reversion results in the enhanced persistence of TBA metabolites via a dynamic exposure regime that defies current fate models and ecotoxicology study designs. Reversion also provides a route to novel steroidal isomers, structural analogs, and derivatives, or "environmental designer steroids," with as-yet-uncharacterized properties and risks. Temperature- and pH-dependent reversion rates also imply substantial uncertainty for nearly all existing TBA metabolite occurrence data. Collectively, these possibilities suggest the unrecognized occurrence of TBA metabolites and/or structurally similar, bioactive transformation products that may contribute to otherwise unexplained observations of endocrine disruption in agriculturally affected receiving waters (*19*, *20*). For example, although chemical analyses often cannot identify causative agents, a recent study indicated widespread (35% of tested waters) androgenic activity in U.S. waters (*21*).

We also recently observed photoproduct-to-parent reversion for dienogest, a potent progestin used as an oral contraceptive (*22*), and for dienedione, an illicit anabolic steroid marketed as a "bodybuilding supplement" (fig. S23). Therefore, it appears that other pharmaceutical steroids, namely those with dienone and trienone moieties, also may exhibit enhanced environmental persistence and pose greater ecological risks than currently realized. In fact, although this work focused solely on phototransformation, we believe that the propensity for reversion is more generally linked to the conjugated enone moiety of TBA metabolites and these other pharmaceuticals. Ultimately, such observations of product-to-parent reversion illustrate that comprehensive assessment of environmental transformation products should be prioritized for high-risk contaminants such as endocrine-disrupting steroids. Further, the use of TBA or similar steroids that are equally prone to environmental transformations that preserve bioactive moieties may need to be reevaluated in favor of more-sustainable pharmaceutical technologies designed to ensure ecosystem protection.

References and Notes

1. K. A. Kidd *et al.*, *Proc. Natl. Acad. Sci. U.S.A.* **104**, 8897–8901 (2007).
2. L. J. Guilette, M. P. Gunderson, *Reproduction* **122**, 857–864 (2001).
3. E. R. Long, D. D. Macdonald, S. L. Smith, F. D. Calder, *Environ. Manage.* **19**, 81–97 (1995).
4. D. E. Latch, J. L. Packer, W. A. Arnold, K. McNeill, *J. Photochem. Photobio. A* **158**, 63–66 (2003).
5. K. Fenner, S. Canonica, L. P. Wackett, M. Elsner, *Science* **341**, 752–758 (2013).
6. B. Schiffer, A. Daxenberger, K. Meyer, H. H. Meyer, *Environ. Health Perspect.* **109**, 1145–1151 (2001).
7. G. T. Ankley *et al.*, *Environ. Toxicol. Chem.* **22**, 1350–1360 (2003).
8. J. D. Lawrence, M. A. Ibarburu, in *Proceedings of the NCCC-134 Conference on Applied Commodity Price Analysis, Forecasting, and Market Risk Management* 16 and 17 April 2007, Chicago; www.farmdoc.illinois.edu/nccc134/conf_2007/pdf/confp05-07.pdf.
9. E. J. Durhan *et al.*, *Environ. Health Perspect.* **114** (suppl. 1), 65–68 (2006).
10. H. E. Gall, S. A. Sassman, L. S. Lee, C. T. Jafvert, *Environ. Sci. Technol.* **45**, 8755–8764 (2011).
11. K. M. Jensen, E. A. Makynen, M. D. Kahl, G. T. Ankley, *Environ. Sci. Technol.* **40**, 3112–3117 (2006).
12. Syntex Animal Health, *Synovex Plus (Trenbolone Acetate and Estradiol Benzoate) Implant Environmental Assessment* (Syntex Animal Health, Palo Alto, CA, for New Animal Drug Application, Center for Veterinary Medicine, FDA, Rockville, MD, 1995); www.fda.gov/ucm/groups/fdagov-public/@fdagov-av-gen/documents/document/ucm072347.pdf.
13. D. G. Cornell, E. Avram, N. Filipescu, *Steroids* **33**, 485–494 (1979).
14. S. Qu, E. P. Kolodziej, D. M. Cwiertny, *Environ. Sci. Technol.* **46**, 13202–13211 (2012).
15. E. P. Kolodziej *et al.*, *Environ. Sci. Technol.* **47**, 5031–5041 (2013).
16. Materials and methods are available as supplementary materials on *Science* Online.
17. R. De Marco, A. Leggio, A. Liguori, F. Perri, C. Siciliano, *Chem. Biol. Drug Des.* **78**, 269–276 (2011).
18. K. R. Stackhouse, C. A. Rotz, J. W. Oltjen, F. M. Mitloehner, *J. Anim. Sci.* **90**, 4656–4665 (2012).
19. V. S. Blazer *et al.*, *Environ. Monit. Assess.* **184**, 4309–4334 (2012).
20. J. K. Leet *et al.*, *Environ. Sci. Technol.* **46**, 13440–13447 (2012).
21. D. A. Stavreva *et al.*, *Sci. Rep* **2**, 937 (2012).
22. M. Oettel, A. Kurischko, *Contraception* **21**, 61–75 (1980).

Acknowledgments: This work was supported by U.S. Department of Agriculture grants 2010-65102-20425 and 2010-65102-20407. NMR instrumentation was supported in part by NIH grant S10-RR025500, with additional support from National Center for Research Resources, NIH, grant UL1RR024979.

LC/MS/MS instrumentation was supported by National Institute of General Medical Sciences, NIH, grant 8 P20 GM103440-11. Computational resources were provided in part by NSF grants CHE-074096, CHE-1039925, and CHE-1044356. Any opinions, findings, conclusions, or recommendations expressed here are those of the authors and do not necessarily represent the official views of sponsoring agencies. The authors acknowledge D. Latch, Y. P. Chin, D. Quilici, J. Bristow, the Sierra Foothill Research and Extension Center and its personnel, and the suggestions of two anonymous reviewers. All data are available in the supplementary materials. The authors declare no conflict of interest.

Supplementary Materials

www.sciencemag.org/content/342/6156/347/suppl/DC1
Materials and Methods
Supplementary Text
Figs. S1 to S23
Tables S1 to S15
References (*23*–*29*)

15 July 2013; accepted 10 September 2013
Published online 26 September 2013;
10.1126/science.1243192

Direct Spectroscopic Characterization of a Transitory Dirhodium Donor-Acceptor Carbene Complex

Katherine P. Kornecki,[1] John F. Briones,[2] Vyacheslav Boyarskikh,[2] Felicia Fullilove,[2] Jochen Autschbach,[3] Kaitlin E. Schrote,[4] Kyle M. Lancaster,[4] Huw M. L. Davies,[2]* John F. Berry[1]*

A multitude of organic transformations catalyzed by dirhodium(II) (Rh_2) complexes are thought to proceed via the intermediacy of highly reactive, electrophilic carbenoid intermediates that have eluded direct observation. Herein, we report the generation of a metastable Rh_2-carbenoid intermediate supported by a donor-acceptor carbene fragment. This intermediate is stable for a period of ~20 hours in chloroform solution at 0°C, allowing for an exploration of its physical and chemical properties. The Rh=C bond, characterized by vibrational and nuclear magnetic resonance spectroscopy, extended x-ray absorption fine structure analysis, and quantum-chemical calculations, has weak σ and π components. This intermediate performs stoichiometric cyclopropanation and C–H functionalization reactions to give products that are identical to those obtained from analogous Rh_2 catalysis.

Isolation of reactive intermediates has historically provided a great deal of insight into the mechanisms of chemical reactions (*1*), and great progress has been made in the synthesis of stable analogs of reactive electron-deficient species such as carbenes and nitrenes (*2*). Carbenoids, or metal-carbene species, first postulated in 1952 (*3*), vary widely in their stability and reactivity. *N*-heterocyclic carbenes (A in Fig. 1), stabilized by two N atoms that flank the carbene C atom, are stable even in the absence of a metal but serve well as unreactive spectator ligands to metals (*4*, *5*). When only one heteroatom is present, the carbene ligand is unstable, but the resulting metal complexes known as Fischer-type carbenes (B in Fig. 1) can be isolated and employed as stoichiometric reagents in reactions such as cyclopropanation (*6*). Schrock-type carbene complexes (C in Fig. 1) have no stabilizing heteroatoms on the carbene carbon and promote catalytic olefin metathesis (*7*). Addition of one or more electron-accepting groups (such as esters) to the carbene center destabilizes it further such that even the metal complexes are often too unstable to isolate (D in Fig. 1). Acceptor carbene complexes are thus often proposed as key intermediates in a broad range of organic reactions. Outstanding among these are Rh_2 tetracarboxylate-catalyzed reactions of donor-acceptor diazocarbonyl compounds, which result in a wide range of synthetically useful transformations (*8*–*18*) (for example, Fig. 1, bottom). Additionally, the initial products of these reactions are often themselves highly reactive and can engage in domino sequences that lead to the rapid construction of complex products (*17*). These systems are catalytically extremely efficient, capable of achieving turnover numbers in excess of 1,000,000 at rates of up to 300 turnovers per second (*14*).

Although some examples of mononuclear metal complexes of acceptor carbenes have been isolated (*19*–*22*), the Rh_2 carbenoid that is featured so prominently in the most efficient and synthetically useful transformations described above has long defied characterization. Our limited understanding of this intermediate has therefore relied on models that rationalize product distributions, computational studies, and limited kinetic studies (*12*, *23*). This type of carbenoid intermediate has remained elusive because, in most instances, its formation is the rate-determining step in the catalytic cycle (*23*). The only known example of an isolated Rh_2 carbene complex is that of the stable nucleophilic Arduengo carbene (*24*), which does not engage in the above-mentioned electrophilic reactivity.

To observe an Rh_2-carbenoid intermediate, we have turned to donor-acceptor diazo esters, in which the donor group is typically aryl or vinyl (*11*, *25*, *26*). Both chemical and computational studies indicate attenuated reactivities for donor-acceptor carbenoids compared with acceptor-only carbenoids, so much so that the C–H functionalization step is predicted to have a similar activation energy to the carbenoid-generation step (*26*). This attenuation not only leads to highly selective transformations and very high catalyst

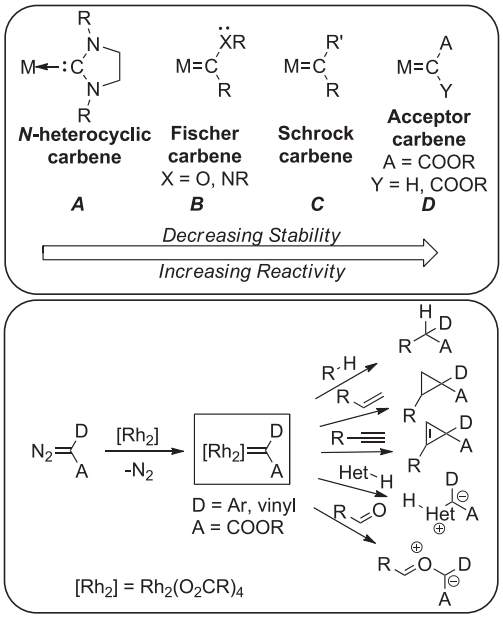

Fig. 1. Metallocarbenoid structure and reactivity. (Top) Classes of metallocarbenoids. M, metal; R, alkyl or aryl. **(Bottom)** Diverse reactions involving dirhodium donor-acceptor carbenoids. Het, heterocycle.

[1]Department of Chemistry, University of Wisconsin–Madison, 1101 University Avenue, Madison, WI 53706, USA. [2]Department of Chemistry, Emory University, 1515 Dickey Drive, Atlanta, GA 30322, USA. [3]Department of Chemistry, University at Buffalo, The State University of New York, Buffalo, NY 14226, USA. [4]Department of Chemistry and Chemical Biology, Baker Laboratory, Cornell University, Ithaca, NY 14853, USA.

*Corresponding author. E-mail: hmdavie@emory.edu (H.M.L.D.); berry@chem.wisc.edu (J.F.B.)

Product-to-Parent Reversion of Trenbolone: Unrecognized Risks for Endocrine Disruption

Shen Qu *et al.*

Science **342**, 347 (2013);
DOI: 10.1126/science.1243192